Research article

Experimental investigation and parameter optimization of Cr₂O₃ atmospheric plasma spray nanocoatings

Seyedmahdi Hashemi [a,*], **Nader Parvin** [b], **Zia Valefi** [c], **Soroush Parvizi** [d]

[a] *Dynamic and Smart Systems Laboratory, Mechanical Industrial and Manufacturing Engineering Department, University of Toledo, OH 43606, USA*

[b] *Department of Materials and Metallurgical Engineering, Amirkabir University of Technology, Tehran, Iran*

[c] *Materials Engineering Research Center, Malek Ashtar University of Technology, Tehran, Iran*

[d] *Materials Engineering Department, Shahid Rajaee Teacher Training University (SRTTU), Tehran, Iran*

A B S T R A C T

In this research, Cr_2O_3 ceramic nano-sized powder particles were prepared using ball milling and then were granulated to reach the proper size for spraying. Afterward, Cr_2O_3 nano-coatings were deposited by atmospheric plasma spraying (APS) process onto stainless steel substrates. To optimize APS parameters, spraying was carried out under six conditions with different parameters. Microstructures of the elemental/milled powder and coatings were characterized via a field emission scanning electron microscope (FESEM) equipped with energy-dispersive spectroscopy (EDS). In this research, Cr_2O_3 coatings were deposited under different spraying conditions to understand the effect of APS parameters on the splat formation, deposition efficiency, and porosities of the coatings. After parameter optimization, spraying was performed under a high deposition efficiency of 46.0±1.3%. The optimized Cr_2O_3 coatings showed porosity content, Knoop microhardness, and adhesive strengths of 8.7±2.2%, 823±27 $HK_{0.2}$, and 49±4 MPa, respectively; making them a good candidate for industrial use.

© 2021 The Authors. Published by Synsint Research Group.

OPEN ACCESS

1. Introduction

Ceramics are generally corrosion-resistant materials with high melting points and brittleness showing low fracture toughness. Regarding the high hardness and low coefficient of friction (COF) of ceramics, they have already been employed as promising candidates for wear applications [1–3].

A straightforward, fast, and low-cost approach to improve the properties of conventional ceramics is producing nanostructured coatings using nano-sized powders. To end this, ball milling has already been employed extensively as a tool to produce ceramic nanopowders [4–7].

Using nanopowders instead of micropowders, decreases the content of structural defects in thermal spray coatings, leading to a more homogeneous structure than conventional coatings (with micro-sized grains). Therefore, nanostructured ceramic coatings due to their bimodal microstructures (fully-melted regions along with partially-melted ones) result in superior mechanical properties in comparison with conventional ones [6, 8–10].

Among thermal spraying methods, the atmospheric plasma spray (APS) process, due to its low cost, high deposition rate, and approved quality of the coatings, has been most developed and attracted researchers' interest since the late 1950s [11, 12]. Moreover, regarding the elevated temperature of plasma flame, almost any ceramics and their composites with high melting points can be melted and deposited on different substrates using the APS process [13–16].
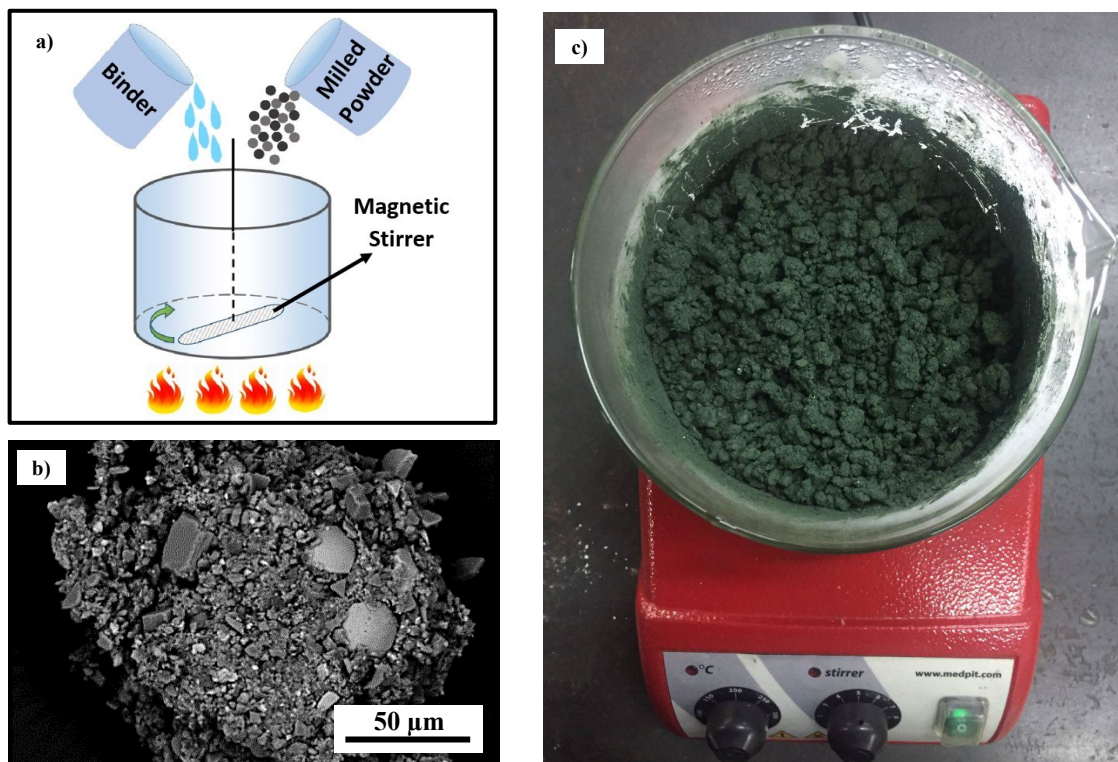
Fig. 1. a) A schematic of granulation process, b) FESEM image of a granulated Cr_2O_3, and c) real photo of granulated Cr_2O_3 powder particles using a magnetic stirrer.

To maintain the nanostructure in the plasma-sprayed coatings, the plasma temperature must be controlled in such a way that it does not rise so high as to cause grain growth (leading to nanostructure loss), nor so low that the material does not melt properly (resulting in coatings with improper cohesion and adhesion to the substrate) [9]. Employing optimum APS parameters, nanostructured coatings with excellent and unique mechanical properties can be achieved [6].

By increasing the initial gas rate (Argon in this research), the velocity of the particles in the plasma flame increases, the melting rate of the powder particles decreases, which totally results in a reduction of deposition efficiency and an increase in the coating porosity [17, 18]. Increasing the amount of secondary gas (Hydrogen in this research) increases the enthalpy and the plasma power. Therefore, the melting rate of the powders leads to a decrease in the coating porosity content [18, 19]. Plasma current has the most significant effect on the porosity of the plasma-sprayed coatings. A decrease in plasma current leads to a reduction in plasma power. As a result, the amount of unmelted or partially melted particles and consequently the porosity of the coating increase. Conversely, high plasma current leads to more melting of the particles and better filling of the coating pores (through the penetration of melt into them) and thus porosity reduction [20]. Increasing the spray distance reduces the velocity and temperature of the particles as they collide with the substrate surface. Therefore, changes in spray distance can significantly affect how the molten particles solidify, the formation of splat, and eventually the final properties of the coatings [21].

Chromium oxide (Cr_2O_3), a high-melting-point and wear/corrosion resistant material, has been so far among the most-demand ones coated by the APS process [22–26].

In the present study, nano-Cr_2O_3 coatings are fabricated using the APS process. Accordingly, their properties such as hardness, surface roughness, splat formation during spraying, and adhesive strength are investigated.

2. Experimental procedure

2.1. Feedstock preparation

In this research, Cr_2O_3 powders with particle size distributions (PSDs) of -70 +20 were used to create the Cr_2O_3 coatings.

Ball milling was carried out via a high-energy tumbler mill model NARYA-MPM 2×250, consisting of two cylindrical containers (capacity: 250 ml) and balls made from hardened steel. Since the 10:1 ratio has already been reported as the optimum ball-to-powder ratio to reach the highest milling efficiency [11], 25 g powder along with 250 g balls were inserted into each container.

Ball milling was performed under an argon atmosphere to avoid powders nitration/oxidation. To achieve nano-sized powders, Cr_2O_3 powder particles were milled for five hours using a high-energy ball milling at its maximum rotation speed of 500 rpm. A particle size analyzer (PSA) was employed to obtain powder PSDs after milling. Milled powder was then granulated using polyvinyl alcohol (PVA) with a powder-to-PVA ratio of 5:1 followed by heating for 10 min at 80 °C to obtain dried granules. Afterward, granulated particles were sieved to reach powder particles with 20–125 μm in diameter size. A schematic of the granulation process, a granulated Cr_2O_3 particle, and the actual image of granulated Cr_2O_3 powders are seen in Fig. 1. As observed, using the PVA as a binder, many small powder particles are
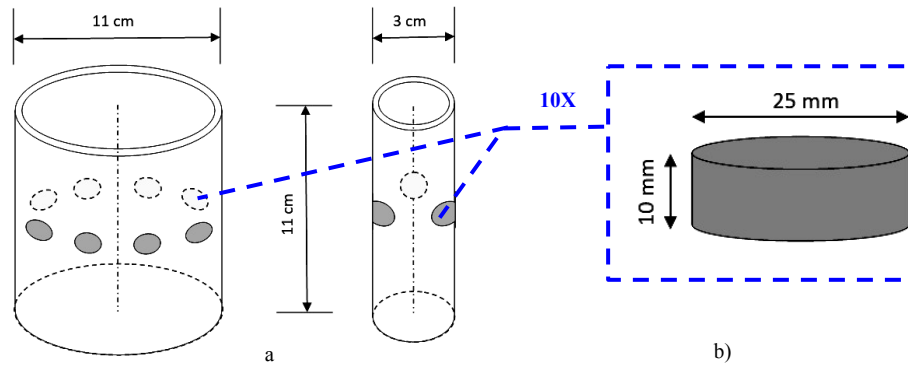
Fig. 2. A schematic of a) large/small holders, b) a disk-shaped substrate.

compacted together to form a bigger particle (Cr_2O_3 granule), appropriate in size for spraying.

2.2. Plasma spraying

APS process was carried out with an F4 Sulzer Metco gun equipped. Before spraying each topcoat, a Ni-5 wt% Al bond-coat (Amdry 956) was sprayed onto a 304L disk-shaped (diameter: 25 mm, height: 10 mm) substrate. To prepare substrates for spraying, they were situated in a large or small holder, respectively holding eight or three substrates, as seen in Fig. 2.

Plasma spraying was carried out under six conditions of C1-C6, as tabulated in Table 1. In plasma spraying, the plasma current, plasma voltage, carrier gas flow rate, powder feeding rate, holder rotating speed, linear gun speed were kept constant for all spraying conditions as 600 A, 57 v, 2.9 l/min, 12 gr/min, 100 rpm, and 7 mm/s, respectively.

Before coating deposition, to obtain acceptable coating adhesion, the surface of the substrates was roughened, cleaned with acetone, grit-blasted with aluminum oxide, and finally cleaned using compressed air and ethanol [27–29]. Mean roughness (average of five linear measurements) of the substrate surface was measured to be around 7.35 μm before spraying, using a Mitutoyo Surftest SJ-201 profilometer.

In thermal spraying, the adhesive strength of coating (coating-to-substrate adhesion) is also affected by residual stress originated from coating solidification. To overcome this problem, substrate preheating should be performed [10, 30, 31]. Accordingly, the substrates were heated up to around 200 °C just before spraying bond-coats.

2.3. Characterization

The microstructure/morphology of the initial powders, granules, and coatings was studied via a field emission scanning electron microscope (FESEM). Furthermore, energy dispersive spectroscopy (EDS) was employed to analyze the phases of powders and coatings.

The glass splat test is a well-known method for considering the formation, flattening, the fraction of splats, and the degree of particle melting in a coating [31–33]. To aim this, a layer of the coating with the same condition as those of main spraying conditions (on 304L substrate) is created on the glass substrate, and then the morphology and formation of the splats are characterized using FESEM. In the present study, the glass splat tests were performed on S6 and S7 coatings.

Phase XRD analyses of the powders/coatings were carried out via the X'PERT PRO MPD instrument (PANalytical, Netherlands), at filament voltage/current of 40 kV/40 mA, using CuK_α radiation(wavelength: 1.54 Å, scan range: 20–90 °, step size: 0.026 °, and scan step time: 48 s.

To calculate the porosities of the coatings, optical microscope images of coating cross-section at 400X magnification were analyzed. This method works based on medical image analysis through a cloud computing approach. Each value of porosity content is the average of ten different analyses.

An OSK 14218-1 (Ogawa Seiki Co.) microhardness tester was used for the Knoop microhardness test. The indentations (load: 200 gr, dwelling time: of 15 s) were employed on the cross-sections of coatings. Each microhardness is the mean value of ten measurements.

The ASTM C633 test method was utilized to determine the bonding strength of coatings. Each strength was the mean value of five measurements.

3. Results and discussion

After milling for five hours, PSDs of Cr_2O_3 powder particles were distributed in the narrow range of 60–80 nm. To overcome the poor flowability of nano-sized powders in the powder feedstock and also to prepare powder particles with proper particle size for spraying

Table 1. Plasma spraying conditions and corresponding parameters.

APS parameter	Spraying condition					
	C1	C2	C3	C4	C5	C6
Spray distance (cm)	11	8	8	10	10	6
Argon gas flow rate (l/min)	65	65	65	45	40	45
Hydrogen gas flow rate (l/min)	10	10	8	8	9	10
Substrate preheating	No	No	No	Yes	Yes	Yes

(10–100 µm), granulation of fine particles is inevitable [6, 9, 12, 34, 35].

Regarding spraying conditions already mentioned in Table 1, the spraying process was accomplished as listed in Table 2.

Deposition efficiency is defined as the mass ratio of the coating to the consumed powder for spraying. Through the deposition efficiency, it can be determined whether the prepared spraying powder is capable of depositing a perfect coating or not [17, 36]. The coating mass, the amount of consumed-powder weight, and therefore the calculated deposition efficiencies in different spraying conditions are tabulated in Table 2. Each value of deposition efficiency is the average of the measurements obtained from three samples of each spraying. Acceptable values of deposition efficiencies and porosities of coatings are highlighted by ticks.

The mean coating thickness was obtained through image analyses done on optical microscopy images of the coating. Each value of coating mass and thickness is the average of ten measurements. Since the too high amount of residual stress at the coating/substrate interface can promote and accelerate the coating fracture or its delamination from the substrate, the thickness of top coatings must preferably be held less than 300 µm [37, 38].

Since the holders move at a constant rotational speed of 100 rpm, the speed ratio of the holders is proportional to their radius; i.e., the linear velocity of the large holder is about 3.67 times that of the small holder. Using large holder, due to the higher linear velocity of spraying, the splats spread more widely, and consequently the coating porosities are less than the coatings created by the small holder. To obtain a certain thickness of coatings, the higher velocity of large holder results in a higher number of spray pass, since coating with less thickness is created on the substrate in each spraying pass (promoting the better spreading of splats in each spray layer).

As mentioned earlier, increasing hydrogen gas flow rate (via increasing the particle temperature) and decreasing argon gas flow rate (via reducing the particle velocity in the plasma flame) increase the melting power of plasma. Increasing the spray distance increases the exposure

time of particles in the plasma environment and, on the other hand, reduces the velocity and temperature of particles when colliding with the substrate, which reduces the fraction of melted and partially-melted particles in the coating, affecting splat formation/solidification.

According to the explanation mentioned above, the first stage of plasma spraying was performed under C1-C3 conditions without substrate preheating, and therefore S1-S3 coatings were deposited. By comparing the metallographic images of the coatings, it was found that the S2 coating (sprayed under C2 conditions) had low porosity. Also, the deposition efficiency of S2 coating was higher than S1 and S3 coatings. As a result, between these spraying conditions, C2 was selected as the optimal one. Fig. 3 shows the FESEM image of the top surface of a typical C2 coating. As seen, the structure of the coatings is composed of molten particles alongside partially-melted or unmelted particles.

Afterward, as the second stage, the argon gas flow rate was reduced to decrease the porosity of S2 coating; meanwhile, the spray distance was increased, and the hydrogen gas flow rate was reduced to increase the exposure time of particles in the plasma flame. As a result, samples S4 and S5 were sprayed under spraying conditions of C4 and C5, respectively. It should be noted that at this stage, coating deposition was performed after preheating the substrates. Also, to improve the properties of S2 coatings, S6 coatings were deposited under C2 condition but this time using the large holder and after preheating the substrate. As seen in Table 2, S6 coatings still had higher efficiency and lower porosity than other coatings. In the last step, spray distance and argon gas flow rate of C2 condition were reduced to obtain the higher deposition efficiency. As expected, S7 coatings with the highest deposition efficiency (about 46%) and the lowest porosity were produced under the spraying condition of C6.

In plasma spraying, the critical plasma spraying parameter (CPSP), as means of comparing the flame temperatures at different spraying conditions, is calculated as below:

$$CPSP = \frac{voltage \times current}{primary\ gas\ flow\ rate} \tag{1}$$

Table 2. Plasma-sprayed coatings deposited under different spraying conditions and the corresponding characteristics.

| Spraying code	Holder size *	Spraying condition	Number of passes	Coating thickness (µm)	Coating mass (gr)	Consumed powder weight (gr)	Deposition efficiency (%)	Porosity content (%)
S1	L	C1	12	120±4	11.00±0.36	77	14.3±0.40	✓ 8.8±2.2
S2	S	C2	3	240±7	5.00±0.15	18	✓ 27.7±0.8	31.5±4.7
S3	S	C3	5	200±7	4.00±0.14	29	13.8±0.5	34.3±6.8
S4	L	C4	42	300±7	29.00±0.68	125	21.0±0.5	✓ 8.3±2.0
S5	S	C5	25	400±11	8.80±0.25	84	10.0±0.3	30.8±5.2
S6	L	C2	18	340±8	32.47±0.75	121	✓ 27.0±0.6	✓ 8.4±2.3
S7	L	C6	28	285±15	27.00±0.74	59	✓ 46.0±1.3	✓ 8.7±2.2

* L: large, S: small
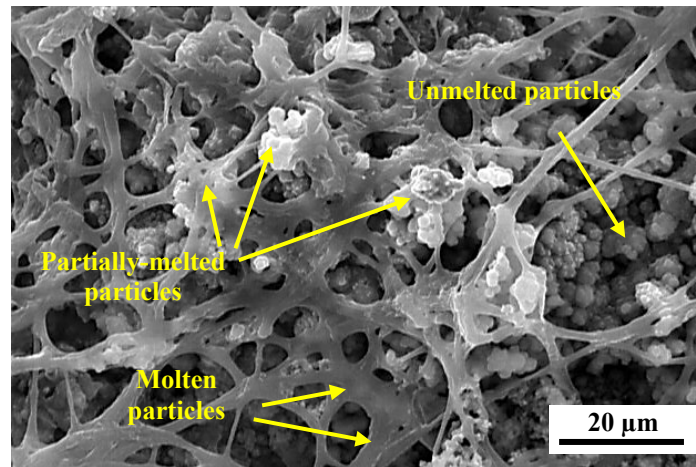
Fig. 3. FESEM image of S2 coatings deposited under C2 spraying condition.

where the measurement units for voltage, current, and primary gas flow rate are volt, ampere, and standard cubic feet per hour (SCFH), respectively. Thus, higher values of CPSP (up to 350–400 V.A.SCFH^{-1}) lead to better coating properties such as higher hardness and wear resistance [7, 39]. Indeed, higher CPSP implies a higher ratio of melted-to-unmelted fractions in the coating, resulting in higher coating consistency [40–42].

In this research, the plasma voltage, current, and argon gas flow rate for S7 coatings are respectively as 57 v, 600 A, and 95.53 SCFH^{-1} (equals to 45 l/min); therefore, according to Eq. 1, CPSP is obtained as

358 V.A.SCFH^{-1}, lying in the appropriate range mentioned earlier. Fig. 4 shows FESEM images of splats and partially-melted particles formed in the glass splat test of Cr_2O_3 coatings produced in the optimal conditions (S6 and S7 coatings). The fraction of molten particles formed in the splat of S7 coating is higher than that in the S6 coating. As a result, it is expected that in S7 coating (created under C6 spray condition), the molten splats more penetrate cavities and fill the pores, leading to a structure with lower porosity and superior mechanical properties. This finding is in agreement with the results already mentioned in Table 2.
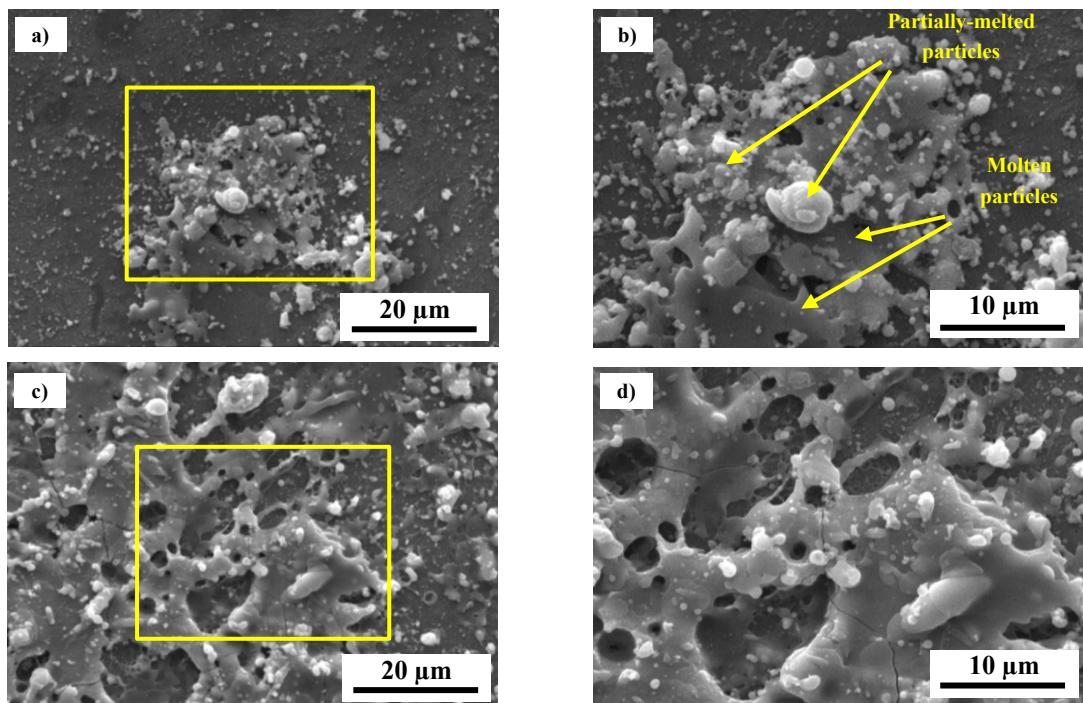

Fig. 4. FESEM images of splats formed in the glass splat test of a, b) S6, and c, d) S7 coatings (yellow box is showing the zoom area).
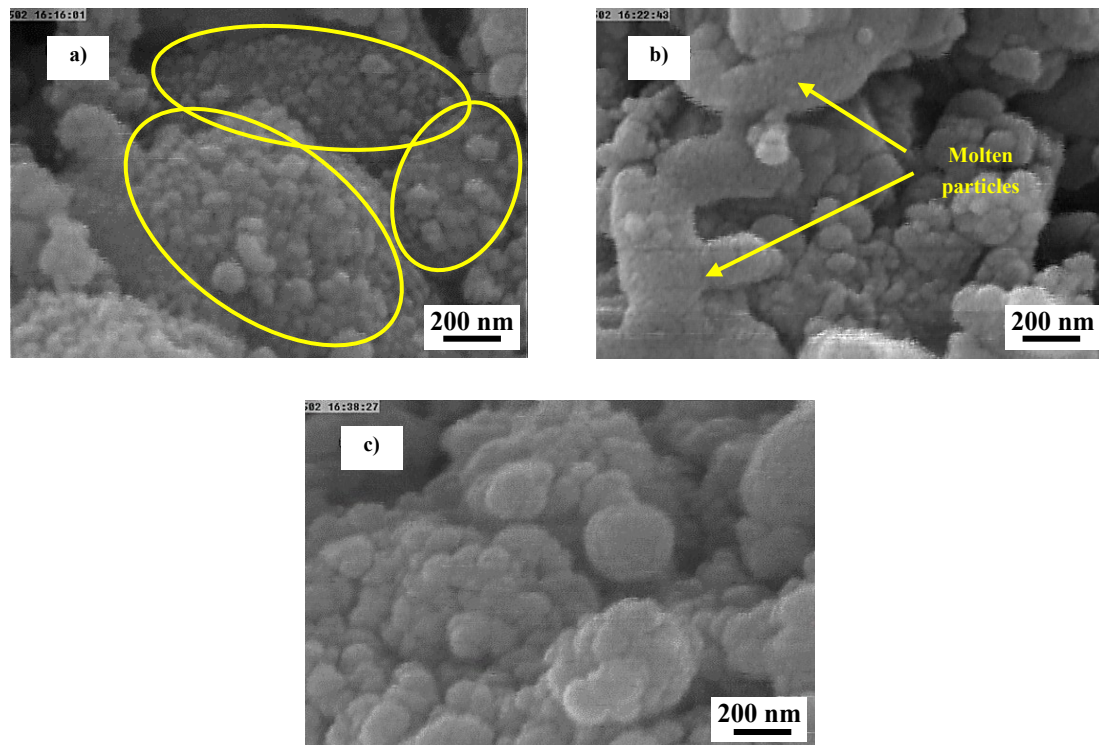
Fig. 5. FESEM morphological images of S1, S2, and S3 samples deposited under C1, C2, and C3 conditions, respectively.

Although the thermal conductivity of a metal substrate and its adhesion to the coatings are different from those of a glass substrate, the glass splat test is still the best way to compare other spraying conditions in terms of quantity/distribution of particles/splats in the coatings and the deposition efficiency [32, 43].

FESEM morphological images of S1, S2, and S3 coatings are shown in Fig. 5. Splats and partially-melted particles are respectively highlighted with yellow arrows and ovals in the figure. As observed, the fraction of melted splats in sample S2 (produced under C2 condition) is higher than the other two samples, resulting in better mechanical properties.

To make it short, in the following, the characteristics of S7 coating (as the optimal one) are illustrated in more detail.

FESEM images of morphologies of S7 coating (Fig. 6) indicate that in plasma spraying of nanopowders, the resulted coatings consist of plenty of micro-sized particles while each microparticle itself is an accumulation of nanoparticles (< 100 nm).

XRD analyses have been performed on the initial/milled Cr_2O_3 powders and the deposited coatings. Regarding the results reported in another paper already published by the authors of this manuscript [44], no new phase (originating from impurity or probable phase transformation) during milling and spraying of the initial powders was detected in the XRD patterns of powders/coating. XRD patterns of the milled powders compared to those of initial powders were broader and shifting toward higher angles due to the increased compressive
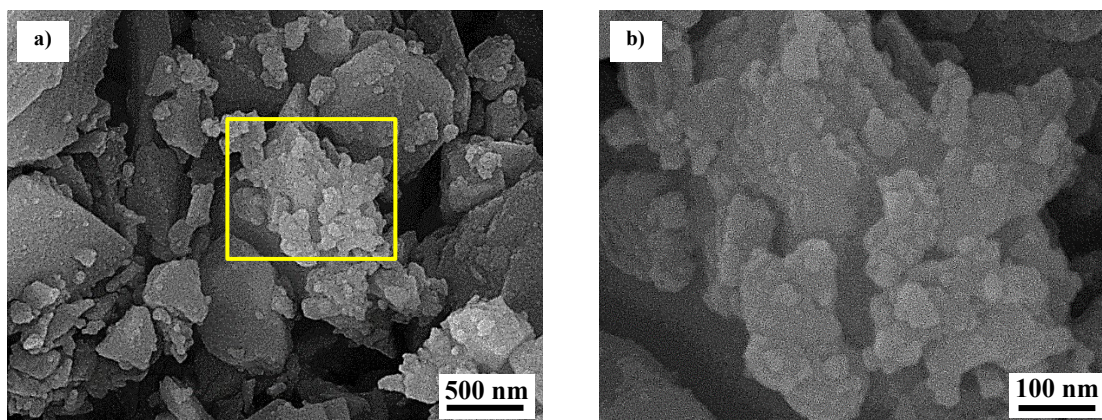

Fig. 6. FESEM morphological images of S7 coating (Fig. 6b is a higher magnification of the yellow box in Fig. 6a).

stress/strain and grain size reduction during milling [5]. The XRD pattern of the optimized S7coating (coded by C coating in the mentioned reference) indicated no new phase or deviation (compared to that of milled powder) appeared in the coating, indicating no solid solution formed during spraying. Coating peaks are broader than milled powder peaks due to the amorphism and grain size reduction of the coating resulting from rapid solidification of melted granulates during spraying [45]. The grain size of the Cr_2O_3 in the S7 coating was calculated to be 54 nm using the Williamson-Hall method through data of (012), (104), (110), and (116) reflections [44]. The results are in agreement with the observation from Fig. 6b.

Regarding the fact that during coating deposition, the space between unmelted particles could not be entirely filled by melted materials, the formation of porosities in plasma-sprayed coatings is unavoidable. Porosities can be formed through air bubbles capturing or evaporating fine particles during spraying owing to the high temperature of the flame. However, coating with low porosity content showing superior mechanical properties is achievable by optimizing process parameters [6, 9]. Considering optical images, the mean porosity fractions of the S7 coatings were calculated to be 8.7±2.2%.

Mean values of Knoop microhardness of S4-S7 coatings were obtained as 541±10, 581±11, 592±14, and 823±27 $HK_{0.2}$, respectively. Nanoceramics generally possess higher hardness rather than conventional ones. However, sometimes high porosity of nanostructured coatings can decrease the hardness value to equal or even lower hardness values compared with conventional coatings [4].

The mean value of bonding strength of S7 coatings is calculated as a high value of 49±4 MPa. More detail on the fracture surface of the coatings during tensile tests has already been reported in Ref. [44]. The higher bonding strength of nanostructured coatings than conventional ones might be related to the higher toughness/strength of nanostructured coatings preventing crack nucleation/propagation in the coating-substrate interface [9]. The fracture surfaces indicated that the coating fractures took place at the topcoat/bond-coat interface, implying the adhesive strength (not cohesive strength) of the coatings [30].

4. Conclusions

In the present work, the authors tried to optimize APS parameters (to have the optimum spraying proficiency) and evaluate the microstructure and the following mechanical properties of nanostructured Cr_2O_3 ceramic coatings deposited onto 304L steel.

No impurity, interaction, or new phase was found during neither ball milling of elemental powders nor spraying the granulated feedstock. Coatings synthesized from nano-sized powders (milled for five hours) possessed nanostructures.

Cr_2O_3 coatings were deposited under six different spraying conditions (C1-C6) to understand the effect of APS parameters on the coating properties. Plasma current/voltage, carrier gas flow rate, powder feeding rate, holder rotating speed, linear gas speed were kept constant for all conditions. Optimized spraying condition is obtained under spray distance, argon gas flow rate, and hydrogen gas flow rate of 6 cm, 45 l/min, and 10 l/min, respectively, using preheated substrates. After parameter optimization, Cr_2O_3 coatings (coded by S7) with a low porosity content of 8.7±2.2% and the highest deposition efficiency (46.0±1.3%) were produced. Optimized Cr_2O_3 coatings showed Knoop microhardness of 823±27 $HK_{0.2}$ and high adhesive strengths of

49±4 MPa. These proper properties of the produced Cr_2O_3 coatings make them appropriate for industrial use.

CRediT authorship contribution statement

Seyedmahdi Hashemi: Writing – original draft, Investigation.
Nader Parvin: Supervision.
Zia Valefi: Methodology.
Soroush Parvizi: Writing – review & editing.

Data availability

The data underlying this article will be shared on reasonable request to the corresponding author.

Declaration of competing interest

The authors declare no competing interests.

Funding and acknowledgment

References

[1] M.M. El Rayes, H.S. Abdo, K.A. Khalil, Erosion -Corrosion of Cermet Coating, Int. J. Electrochem. Sci. 8 (2013) 1117–1137. https://doi.org/10.1016/S1452-3981(23)14085-5.

[2] W.M. Rainforth, The wear behaviour of oxide ceramics-A Review, J. Mater. Sci. 39 (2004) 6705–6721. https://doi.org/10.1023/B:JMSC.0000045601.49480.79.

[3] A. Tiwari, R.A. Gerhardt, M. Szutkowska, Advanced Ceramic Materials, Wiley-Scrivener. (2016). https://doi.org/10.1002/9781119242598.

[4] Z.Z. Fang, H. Wang, Sintering of ultrafine and nanosized ceramic and metallic particles, Ceramic Nanocomposites, Woodhead Publishing. (2013) 431–473.

[5] C. Suryanarayana, T. Klassen, E. Ivanov, Synthesis of nanocomposites and amorphous alloys by mechanical alloying, J. Mater. Sci. 46 (2011) 6301–6315. https://doi.org/10.1007/s10853-011-5287-0.

[6] V. Chawla, B. Sidhu, D. Puri, S. Prakash, Performance of plasma sprayed nanostructured and conventional coatings, J. Aust. Ceram. Soc. 44 (2008) 56–62.

[7] M. Gell, E.H. Jordan, Y.H. Sohn, D. Goberman, L. Shaw, T.D. Xiao, Development and implementation of plasma sprayed nanostructured ceramic coatings, Surf. Coat. Technol. 146–147 (2001) 48–54. https://doi.org/10.1016/S0257-8972(01)01470-0.

[8] D. Ghosh, A.K. Shukla, H. Roy, Nano Structured Plasma Spray Coating for Wear and High Temperature Corrosion Resistance Applications, J. Inst. Eng. (India): D. 95 (2014) 57–64. https://doi.org/10.1007/s40033-014-0034-8.

[9] R.S. Lima, B.R. Marple, Thermal Spray Coatings Engineered from Nanostructured Ceramic Agglomerated Powders for Structural, Thermal Barrier and Biomedical Applications: A Review, J. Therm. Spray Technol. 16 (2007) 40–63. https://doi.org/10.1007/s11666-006-9010-7.

[10] N.B. Dahotre, S. Nayak, Nanocoatings for engine application, Surf. Coat. Technol. 194 (2005) 58–67. https://doi.org/10.1016/j.surfcoat.2004.05.006.

[11] R.F. Bunshah, Handbook of Hard Coatings: Deposition Technologies, Properties and Applications, William Andrew Pub., Park Ridge, N.J., Norwich, N.Y. (2001).

[12] A. Cellard, V. Garnier, G. Fantozzi, G. Baret, P. Fort, Wear resistance of chromium oxide nanostructured coatings, Ceram. Int. 35 (2009) 913–916. https://doi.org/10.1016/j.ceramint.2008.02.022.

[13] G.E. Kim, M. Brochu, Thermal spray nanostructured ceramic and metal-matrix composite coatings, Anti-Abrasive Nanocoatings, Woodhead Publishing. (2015) 481–511. https://doi.org/10.1016/B978-0-85709-211-3.00019-4.

[14] G. Bolelli, V. Cannillo, L. Lusvarghi, T. Manfredini, Wear behaviour of thermally sprayed ceramic oxide coatings, Wear. 261 (2006) 1298–1315. https://doi.org/10.1016/j.wear.2006.03.023.

[15] A. Vardelle, C. Moreau, N.J. Themelis, C. Chazelas, A Perspective on Plasma Spray Technology, Plasma Chem. Plasma Process. 35 (2015) 491–509. https://doi.org/10.1007/s11090-014-9600-y.

[16] A. Wank, B. Wielage, G. Reisel, T. Grund, E. Friesen, Performance of Thermal Spray Coatings under Dry Abrasive Wear Conditions, 4th Int. Conf. THE Coatings, Erlangen. 4 (2004).

[17] Y.J. Wang, J.Y. Xu, Q.H. Zhao, Y. Wang, B. Gao, Effects of various power process parameters on deposition efficiency of plasma-sprayed Al2O3-40% wt. TiO₂ coatings, IOP Conference Series: Mater. Sci. Eng. 213 (2017) 012042. https://doi.org/10.1088/1757-899X/213/1/012042.

[18] F. Gao, X. Huang, R. Liu, Q. Yang, Optimization of Plasma Spray Process Using Statistical Methods, J. Therm. Spray Technol. 21 (2012) 176–186. https://doi.org/10.1007/s11666-011-9700-7.

[19] A. Scrivani, G. Rizzi, C.C. Berndt, Enhanced thick thermal barrier coatings that exhibit varying porosity, Mater. Sci. Eng.: A. 476 (2008) 1–7. https://doi.org/10.1016/j.msea.2007.04.035.

[20] D. Thirumalaikumarasamy, K. Shanmugam, V. Balasubramanian, Influences of atmospheric plasma spraying parameters on the porosity level of alumina coating on AZ31B magnesium alloy using response surface methodology, Prog. Nat. Sci.: Mater. 22 (2012) 468–479. https://doi.org/10.1016/j.pnsc.2012.09.004.

[21] J.M. Guilemany, J. Nin, Thermal spraying methods for protection against wear, Surface Coatings for Protection against Wear, Woodhead Publishing. (2006) 249–301. https://doi.org/10.1533/9781845691561.249.

[22] P. Ctibor, I. Píš, J. Kotlan, Z. Pala, I. Khalakhan, et al., Microstructure and Properties of Plasma-Sprayed Mixture of Cr₂O₃ and TiO₂, J. Therm. Spray Technol. 22 (2013) 1163–1169. https://doi.org/10.1007/s11666-013-9969-9.

[23] M. Szafarska, J. Iwaszko, Laser Remelting Teratment of Plasma-Sprayed Cr₂O₃ Oxide Coatings, Arch. Metall. Mater. 57 (2012). https://doi.org/10.2478/v10172-012-0013-8.

[24] Y. Sert, N. Toplan, Tribological behavior of a plasma-sprayed Al₂O₃-TiO₂-Cr₂O₃ coating, Mater. Tehnol. 47 (2013) 181–183.

[25] S.M. Hashemi, N. Parvin, Z. Valefi, Effect of microstructure and mechanical properties on wear behavior of plasma-sprayed Cr₂O₃-YSZ-SiC coatings, Ceram. Int. 45 (2019) 5284–5296. https://doi.org/10.1016/j.ceramint.2018.11.226.

[26] S.M. Hashemi, N. Parvin, Z. Valefi, M. Alishahi, Comparative study on tribological and corrosion protection properties of plasma sprayed Cr₂O₃-YSZ-SiC ceramic coatings, Ceram. Int. 45 (2019) 21108–21119. https://doi.org/10.1016/j.ceramint.2019.07.087.

[27] J.R. Davis, Handbook of Thermal Spray Technology, ASM International. (2004).

[28] M.K. Singla, H. Singh, V. Chawla, Thermal Sprayed CNT Reinforced Nanocomposite Coatings – A Review, J. Miner. Mater. Charact. Eng. 10 (2011) 20904. https://doi.org/10.4236/jmmce.2011.108056.

[29] K.E. Schneider, V. Belashchenko, M. Dratwinski, S. Siegmann, A. Zagorski, Thermal Spraying for Power Generation Components, Wiley-VCH Verlag GmbH & Co. KGaA. (2006). https://doi.org/10.1002/3527609342.

[30] K. Yang, X. Zhou, C. Liu, S. Tao, C. Ding, Sliding Wear Performance of Plasma-Sprayed Al2O3-Cr2O3 Composite Coatings Against Graphite under Severe Conditions, J. Therm. Spray Technol. 22 (2013). 1154–1162. https://doi.org/10.1007/s11666-013-9959-y.

[31] S. Chandra, P. Fauchais, Formation of Solid Splats during Thermal Spray Deposition, J. Therm. Spray Technol. 18 (2009) 148–180. https://doi.org/10.1007/s11666-009-9294-5.

[32] R. Gadow, A. Killinger, C. Li, Product Development with Thermally Sprayed Functional Coatings on Glass and Glass–Ceramics Substrates, Int. J. Appl. Ceram. Technol. 2 (2005) 493–503. https://doi.org/10.1111/j.1744-7402.2005.02050.x.

[33] R. Gadow, A. Killinger, C. Li, Plasma Sprayed Ceramic Coatings on Glass and Glass Ceramic Substrates, Innovative Processing and Synthesis of Ceramics, Glasses, and Composites V, John Wiley & Sons, Ltd. 129 (2006) 15–30. https://doi.org/10.1002/9781118370872.ch2.

[34] D.J. Green, An Introduction to the Mechanical Properties of Ceramics, Cambridge University Press, Cambridge. (1998). https://doi.org/10.1017/CBO9780511623103.

[35] P. Fauchais, G. Montavon, G. Bertrand, From Powders to Thermally Sprayed Coatings, J. Therm. Spray Technol. 19 (2010) 56–80. https://doi.org/10.1007/s11666-009-9435-x.

[36] A. Behera, Prediction and Analysis of Deposition Effeciency of Plasma Spray Coating Using Artificial Intelligent Method, Open J. Compos. Mater. 2 (2012) 54–60. https://doi.org/10.4236/ojcm.2012.22008.

[37] R. Gadow, M.J. Riegert-Escribano, M. Buchmann, Residual stress analysis in thermally sprayed layer composites, using the hole milling and drilling method, J. Therm. Spray Technol. 14 (2005) 100. https://doi.org/10.1361/10599630522756.

[38] C. Li, X. Zhang, Y. Chen, J. Carr, S. Jacques, et al., Understanding the residual stress distribution through the thickness of atmosphere plasma sprayed (APS) thermal barrier coatings (TBCs) by high energy synchrotron XRD; digital image correlation (DIC) and image based modelling, Acta Mater. 132 (2017) 1–12. https://doi.org/10.1016/j.actamat.2017.03.044.

[39] Y. Feng, T. Zhang, Determination of fracture toughness of brittle materials by indentation, Acta Mechanica Solida Sinica. 28 (2015) 221–234. https://doi.org/10.1016/S0894-9166(15)30010-0.

[40] V. Bolleddu, V. Racherla, P.P. Bandyopadhyay, Microstructural characterization of plasma sprayed conventional and nanostructured coatings with nitrogen as primary plasma gas, Surf. Coat. Technol. 235 (2013) 424–432. https://doi.org/10.1016/j.surfcoat.2013.07.069.

[41] V.P. Singh, A. Sil, R. Jayaganthan, Wear of Plasma Sprayed Conventional and Nanostructured Al₂O₃ and Cr₂O₃, Based Coatings, Trans. Indian Inst. Met. 65 (2011) 1–12. https://doi.org/10.1007/s12666-011-0070-0.

[42] D. Goberman, Microstructure investigation of plasma sprayed alumina 13 weight percent titania coatings from nanocrystalline feed powders, ETD Collection for University of Connecticut, Storrs, Connecticut. (2002).

[43] H. Fukanuma, R. Huang, Y. Tanaka, Y. Uesugi, Mathematical Modeling and Numerical Simulation of Splat Cooling in Plasma Spray Coatings, J. Therm. Spray Technol. 18 (2009) 965. https://doi.org/10.1007/s11666-009-9366-6.

[44] S.M. Hashemi, N. Parvin, Z. Valefi, Effect of Addition of Multimodal YSZ and SiC Powders on the Mechanical Properties of Nanostructured Cr₂O₃ Plasma-Sprayed Coatings, J. Therm. Spray Technol. 28 (2019) 544–562. https://doi.org/10.1007/s11666-019-00834-8.

[45] S. Liu, Y. Zhu, X. Lai, X. Zheng, R. Jia, X. Yuan, Influence of Different Heat Treatment Temperatures on the Microstructure, Corrosion, and Mechanical Properties Behavior of Fe-Based Amorphous/Nanocrystalline Coatings, Coatings. 9 (2019) 858. https://doi.org/10.3390/coatings9120858.